ACS OMEGA

http://pubs.acs.org/journal/acsodf

Article

Conjugation of Carboxylated Graphene Quantum Dots with Cecropin P1 for Bacterial Biosensing Applications

Jonathan A. Bruce* and Jude C. Clapper

Cite This: https://dx.doi.org/10.1021/acsomega.0c03342

Read Online

ACCESS | Metrics & More | Article Recommendations | Supporting Information

ABSTRACT: Biosensors that can accurately and rapidly detect bacterial concentrations in solution are important for potential applications such as assessing drinking water safety. Meanwhile, quantum dots have proven to be strong candidates for biosensing applications in recent years because of their strong light emission properties and their ability to be modified with a variety of functional groups for the detection of different analytes. Here, we investigate the use of conjugated carboxylated graphene quantum dots (CGQDs) for the detection of *Escherichia coli* using a biosensing assay that focuses on measuring changes in fluorescence intensity. We have further developed this assay into a novel, compact, field-deployable biosensor focused on rapidly measuring changes in absorbance to determine *E. coli* concentrations. Our CGQDs were conjugated with cecropin P1, a naturally produced antibacterial peptide that facilitates the attachment of CGQDs to *E. coli* cells; to our knowledge, this is the first instance of cecropin P1 being used as a biorecognition element for quantum dot biosensors. As such, we confirm the structural modification of these conjugated CGQDs in addition to analyzing their optical characteristics. Our findings have the potential to be used in situations where rapid, reliable detection of bacteria in liquids, such as drinking water, is required, especially given the low range of *E. coli* concentrations (10^3 to 10^6 CFU/mL) within which our two biosensing assays have collectively been shown to function.

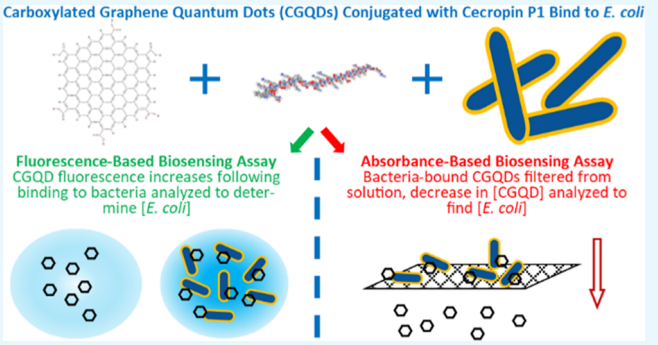

1. INTRODUCTION

Biosensing assays are important for detecting disease-causing microorganisms that may be present in consumables and for determining their concentrations.[1−3] One such microorganism is *Escherichia coli* O157:H7, a Shiga toxin-producing strain of *E. coli* that can cause severe, potentially fatal conditions such as hemolytic uremic syndrome upon ingestion.[4]

In recent years, many quantum dot-based biosensing assays for the detection of *E. coli* have been developed.[5,6] These biosensors often rely on measuring changes in the quantum dots' absorbance, fluorescence, or electrochemical properties when they interact with a given analyte, in this case *E. coli* cells. A table of selected publications on quantum dot biosensors for *E. coli* and their stated limits of detection (LOD) is shown below (Table 1).

As seen in Table 1, current quantum dot biosensors designed for *E. coli* detection generally have good sensitivity and specificity, but many utilize heavy-metal quantum dots containing elements like cadmium and may therefore present potential hazards regarding their usage and disposal, given the potential for Cd^{2+} leaching.[19−21]

Therefore, in this study, we aim to create a simple, nontoxic, and rapid fluorescence-based quantum dot biosensing assay that utilizes fluorescence spectroscopy for the detection and quantification of *E. coli* in solution. In addition, we aim to go beyond this laboratory-based assay to develop a rapid, portable, absorbance-based biosensing assay for detecting *E. coli* concentrations in liquids. Moreover, we have developed novel, modified quantum dots for use in these biosensing assays, which consist of carboxylated graphene quantum dots (CGQDs) conjugated with cecropin P1, a cationic antibacterial peptide containing 31 amino acids with 10 free amines.

Graphene quantum dots were chosen for this study because of their low biotoxicity[22] and strong fluorescence,[23,24] which are important characteristics to ensure the safety and efficacy of the assay, respectively. Meanwhile, cecropin P1 was chosen as a biorecognition element of our quantum dots because of its ability to bind to *E. coli* cell walls as a part of its action mechanism[25,26] since ensuring CGQD−*E. coli* attachment is a key part of how our biosensing assays function.

The attachment of the CGQDs to the cecropin P1 is hypothesized to occur via the attachment of carboxyl groups

Received: July 12, 2020
Accepted: September 25, 2020

Table 1. Overview of Current Quantum Dot Biosensors for the Detection of *E. coli* and Their Stated LODs/Concentration Ranges Tested

assay type	quantum dots	LOD	linear detection range/range tested
electrochemical (sandwich-type assay)[7]	CdS QDs encapsulated in ZIF-8 metal−organic framework	3 CFU/mL	10^1 to 10^8 CFU/mL
fluorescence/immunomagnetic separation[8]	streptavidin-conjugated CdSe−ZnS QDs	10^3 CFU/mL	10^3 to 10^7 CFU/mL
electrochemiluminescence[9]	nitrogen-doped GQDs	8 CFU/mL	10^1 to 10^7 CFU/mL
fluorescence (ELISA direct-type assay)[10]	CdTe core/CdS shell QDs	not explicitly stated	$\sim 10^{2.5}$ to 10^6 CFU/mL
fluorescence (immunochromatography test strips)[11]	CdTe/CdS quantum dots	10^4 CFU/mL	10^2 to 10^9 CFU/mL (detection demonstrated for 10^4 CFU/mL and above)
fluorescence (ELISA sandwich-type assay)[12]	carboxylated CdSe/ZnS QDs	10^2 CFU/mL	10^2 to 10^5 CFU/mL
fluorescence[13]	mannose-modified carbon QDs	450 CFU/mL	10^2 to 10^8 CFU/mL
fluorescence[14]	colistin-modified carbon QDs	460 CFU/mL	3.81×10^2 to 2.44×10^4 CFU/mL
fluorescence[15]	amikacin-modified carbon QDs	552 CFU/mL	7.625×10^2 to 3.904×10^5 CFU/mL
fluorescence/magnetic separation[16]	chitosan-functionalized magnetic nanoparticles bound to carbon quantum dots	3.5×10^2 CFU/mL	3.5×10^2 to 2.9×10^3 CFU/mL
fluorescence (ELISA sandwich-type assay)[17]	carboxylated CdSe/ZnS core−shell QDs conjugated with antirabbit IgG	1 CFU/mL	$1-10^5$ CFU/mL
fluorescence[18]	colistin-functionalized CdSe/ZnS QDs	28 CFU/mL	1.3×10^2 to 1.0×10^3 CFU/mL

on the CGQDs' edge structure to the amine groups present on cecropin P1. Such formation of amide bonds is possible in the presence of *N*-hydroxysuccinimide (NHS) and 1-ethyl-3-(3-dimethylaminopropyl)carbodiimide (EDC), which activate the CGQDs' carboxyl groups so that the conjugation reaction can take place.

The solutions necessary for our biosensing assays can be prepared in relatively rapid, room-temperature reactions, which is an advantage for potential applications.

For our fluorescence-based biosensing assay, we used a plate reader to quantify changes in conjugated CGQD fluorescence associated with CGQD−*E. coli* interactions. We hypothesize that the main factor responsible for the observed changes in fluorescence is the attachment of the bacteria to the conjugated CGQDs, which could affect fluorescence-related characteristics of the quantum dots such as band gap width. The occurrence of conjugated CGQD−*E. coli* binding is suggested by the action mechanism of cecropin P1, namely its ability to bind to cell walls of Gram-negative bacteria.

For our absorbance-based biosensing assay, we used optical density measurements to quantify the amount of conjugated CGQDs bound to *E. coli* cells following thorough mixing, which then allowed us to calculate the concentration of *E. coli* cells in solution. In this assay, absorbance was used as an indicator of conjugated CGQD concentration, with changes in CGQD absorbance corresponding to changes in CGQD concentration. The spectrophotometer used for obtaining absorbance measurements in this assay is compact and lightweight, making this setup more ideal for portable use than our fluorescence-based assay, which utilizes a bench top plate reader.

2. RESULTS AND DATA

2.1. Fluorescence Spectra for CGQDs and Cecropin P1-Conjugated CGQDs. Figure 1a depicts the fluorescence spectra for nonconjugated CGQDs (yellow) and CGQDs following cecropin P1 conjugation (blue). Both spectra were measured using an excitation wavelength of 400 nm.

As can be seen from the spectra in Figure 1a, CGQD conjugation with cecropin P1 results in significant fluorescence quenching. This quenching was quantified in Figure 1b, which shows the differences in fluorescence intensity between conjugated and nonconjugated CGQDs; a negative difference indicates fluorescence quenching.

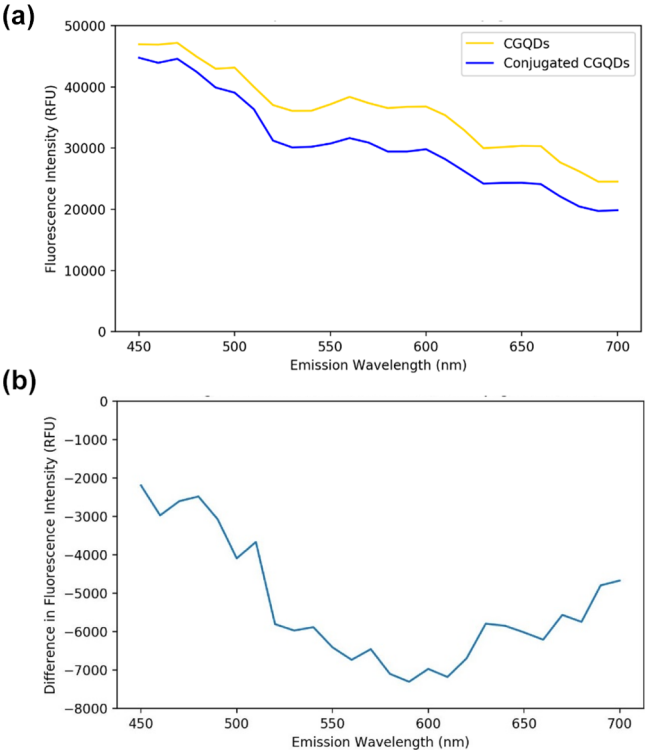

Figure 1. (a) Fluorescence spectra for nonconjugated CGQDs (yellow) and conjugated CGQDs (blue). All measurements taken with excitation wavelength = 400 nm. (b) Change in fluorescence intensity between conjugated CGQDs and nonconjugated CGQDs. All measurements taken with excitation wavelength = 400 nm. The quenching (potentially ACQ) observed following conjugation indicates that the CGQDs have successfully been conjugated with cecropin P1.

2.2. Absorbance Spectra for CGQDs and Cecropin P1-Conjugated CGQDs. In order to analyze changes in CGQDs' optical properties due to conjugation with cecropin P1, absorbance spectra of CGQDs (yellow) and conjugated CGQDs (blue) were measured at equal concentrations, as

https://dx.doi.org/10.1021/acsomega.0c03342
ACS Omega XXXX, XXX, XXX−XXX

shown in Figure 2. As can be seen from the spectra, there is a red shift of 10 nm following cecropin conjugation and a significant increase in absorbance values.

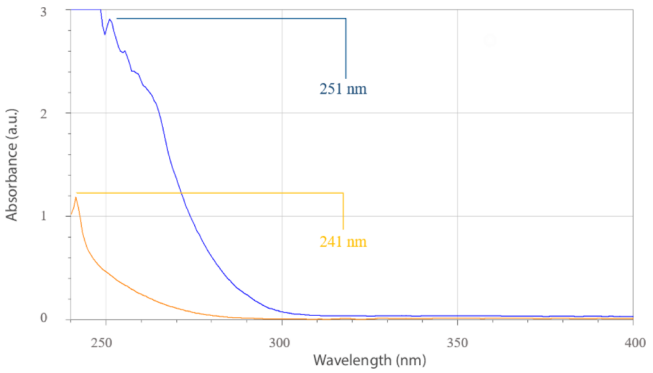

Figure 2. Absorbance spectra for nonconjugated CGQDs (yellow) and cecropin P1-conjugated CGQDs (blue), at equal concentrations. As can be seen in the spectra, conjugation with cecropin P1 results in a red shift of 10 nm and an increase in absorbance values.

Furthermore, an absorbance spectrum of pure cecropin P1 solution (Figure S1) confirmed that any residual cecropin from the conjugation procedure would have a negligible impact on absorbance values. Therefore, the observed increase in absorbance values results from changes in CGQD absorbance due to conjugation with cecropin P1, rather than the presence of residual reactants from the conjugation procedure.

2.3. Transmission Electron Microscope Imaging of CGQDs, Cecropin P1, and Cecropin P1-Conjugated CGQDs. Transmission electron microscope imaging, as shown in Figure 3, was performed in order to provide further proof of CGQD conjugation with cecropin P1.

Figure 3a represents a transmission electron microscopy (TEM) image of nonconjugated CGQDs, which were used as received from the manufacturer (dissolved in water at a concentration of 1 mg/mL prior to TEM sample preparation and imaging). In the image, several CGQDs approximately 10 nm in size can be observed. This corresponds well with both the size distribution (5−10 nm) and the sample TEM image provided in the manufacturer's technical data (please see Experimental Methods for more information).

Meanwhile, Figure 3b represents a TEM image of cecropin P1 peptides, dissolved in water at a concentration of ∼0.050 mg/mL prior to TEM sample preparation and imaging. In the image, a cluster of several cecropin P1 peptides ranging from approximately 20 to 30 nm in size can be observed. These peptides correspond well in appearance with other previously published TEM images of cecropin P1.[27]

Finally, Figure 3c represents a TEM image of cecropin P1-conjugated CGQDs, dissolved in water at a concentration of ∼0.075 mg/mL prior to TEM sample preparation and imaging. The image shows a CGQD approximately 10 nm in size bound to several cecropin P1 peptides (the exact number of peptides is undetermined). Because of similarities in size, shape, and coloration with the CGQDs shown in Figure 3a and the peptides shown in Figure 3b, the TEM image shown in Figure 3c suggests that conjugation of CGQDs with cecropin P1 peptides has taken place as a result of our conjugation protocol.

2.4. Fluorescence-Based Assay: Change in Fluorescence Versus *E. coli* Concentration. Our first biosensing

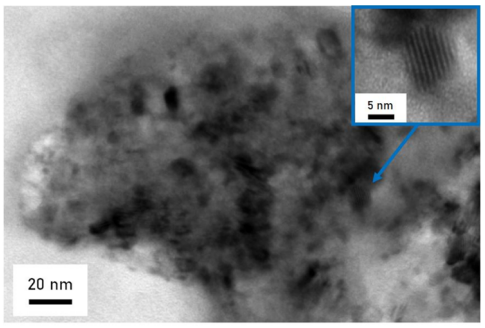

(a) Carboxylated GQDs (CGQDs)

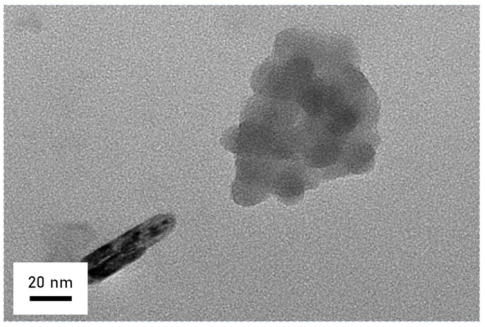

(b) Cecropin P1

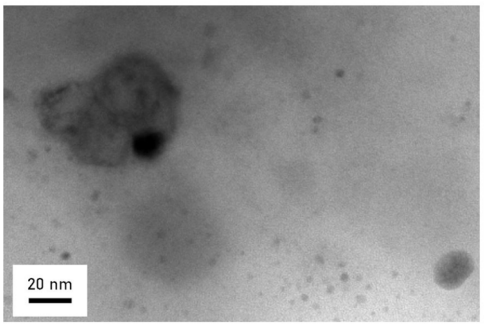

(c) Cecropin P1-Conjugated CGQDs

Figure 3. TEM images of (a) CGQDs, (b) cecropin P1, and (c) conjugated CGQDs. Image (a) shows concentrated CGQDs (1 mg/mL) approximately 10 nm in size. Image (b) shows cecropin P1 peptides (∼0.050 mg/mL) approximately 20−30 nm in size. Meanwhile, image (c) shows an image of a conjugated CGQD sample (∼0.075 mg/mL), depicting a CGQD bound to cecropin P1 peptides. The number of cecropin P1 peptides that can bind to CGQDs is variable, and it is unclear how many peptides have bound to the CGQD shown in image (c).

assay relies on analyzing CGQD fluorescence intensity in relation to *E. coli* concentration. The fluorescence of CGQDs can change when CGQD−*E. coli* binding occurs, a process facilitated by CGQD conjugation with cecropin P1. Analyzing these changes in fluorescence can help determine the amount of *E. coli* bound to CGQDs, and therefore the amount of *E. coli* present in a sample.

Figure 4 depicts the changes in fluorescence that result from mixing conjugated CGQDs with resuspended *E. coli* liquid cultures of various concentrations. As can be seen in the graph, the fluorescence of the conjugated CGQDs increases when they are mixed with *E. coli* concentrations ranging between 1.56×10^4 and 1.56×10^6 CFU/mL. Furthermore, the relationship between fluorescence and *E. coli* concentration can be described quantitatively by the four-parameter logistic curve

https://dx.doi.org/10.1021/acsomega.0c03342
ACS Omega XXXX, XXX, XXX−XXX

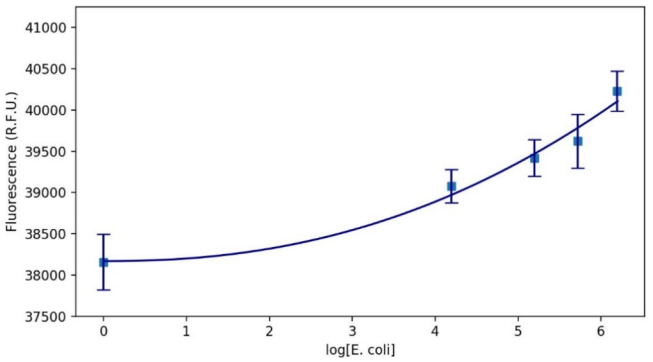

Figure 4. Fluorescence intensity of conjugated CGQD samples after mixing with various concentrations of *E. coli* cells. Fluorescence intensity measurements taken using $\lambda_{excitation}$ = 400 nm and $\lambda_{emission}$ = 640 nm. Data correspond to the mean and 95% confidence interval of measurements from six independent trials, with any outliers removed by the 1.5 × IQR rule. Curve fitted according to the four-parameter logistic function,[28] with R^2 of the fit equal to 0.9763.

fit shown in Figure 4.[28] This model demonstrated excellent fit with our data, and therefore our assay allows for the precise determination of *E. coli* concentration in a given sample from fluorescence intensity measurements.

Meanwhile, Figure 5 depicts the changes in fluorescence that result from mixing nonconjugated CGQDs with resuspended

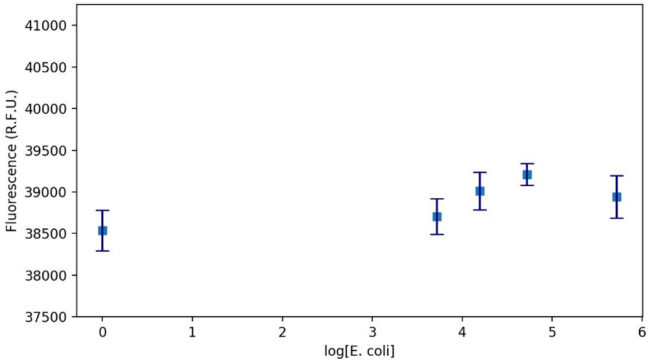

Figure 5. Fluorescence intensity of nonconjugated CGQD samples after mixing with various concentrations of *E. coli* cells. Fluorescence intensity measurements taken using $\lambda_{excitation}$ = 400 nm and $\lambda_{emission}$ = 640 nm. Data correspond to the mean and 95% confidence interval of measurements from six independent trials, with any outliers removed by the 1.5 × IQR rule. No fit performed on the data, which do not appear to follow the four-parameter logistic trend observed in Figure 4.

E. coli liquid cultures of various concentrations. As can be seen when comparing Figures 5 to 4, nonconjugated CGQDs produce much less significant increases in fluorescence intensity when mixed with comparable concentrations of *E. coli* compared with conjugated CGQDs. Moreover, these increases do not appear to follow the same trend (four-parameter logistic curve) observed in Figure 4. Therefore, conjugation of CGQDs with cecropin P1 appears to be essential for the detection of *E. coli* with our fluorescence-based biosensing assay.

It is worth noting that there may be some nonspecific interactions between nonconjugated CGQDs and *E. coli* that may explain some of the small fluorescence increases observed in Figure 5. However, it is clear from the differences between the figures that this nonspecific binding is insignificant compared to binding between conjugated CGQDs and *E. coli* cells.

All measurements for both Figures 4 and 5 were performed using an excitation wavelength of 400 nm and an emission wavelength of 640 nm. The data shown in both figures correspond to the mean and 95% confidence intervals of measurements from six independent trials performed on the same day. Any outlier fluorescence intensity data were removed (as determined by the 1.5 × IQR rule) to mitigate their effects on calculations of mean and 95% confidence intervals. The *y*-axes of both figures are identically scaled to facilitate direct comparisons between the two.

2.5. Absorbance-Based Assay: Change in Absorbance Versus *E. coli* Concentration. Our second biosensing assay relies on analyzing the absorbance of CGQDs unbound to *E. coli* in a sample in relation to *E. coli* concentration. Based on these absorbance measurements, the concentration of unbound CGQDs can be quantified, allowing the determination of *E. coli* concentration in a sample. This test was performed to demonstrate how our CGQDs could be used in a more convenient biosensing assay design, as the spectrophotometer used here is much smaller and less expensive than the plate reader used in our fluorescence-based assay.

Figure 6 depicts the decreases in absorbance of conjugated CGQD samples, measured relative to a control sample, after

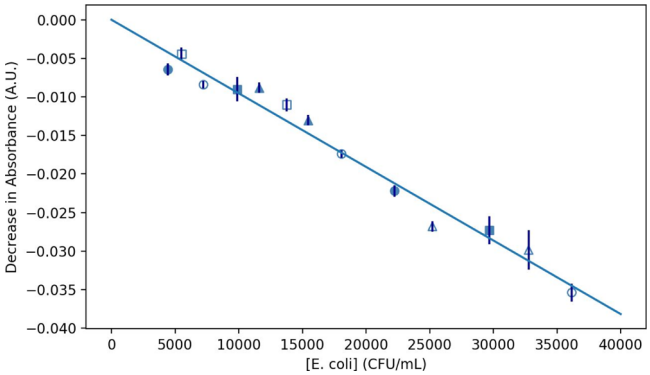

Figure 6. Decrease in the absorbance of conjugated CGQDs after being mixed with *E. coli* and filtered through a 0.22 μm filter. Absorbance measurements taken at 450.0 nm. Data correspond to measurements from six independent trials, with different icons representing different trials. Error bars correspond to the 95% confidence interval of measurements taken on the same sample at five random time points to mitigate the effects of machine uncertainty and random data fluctuations. Curve fitted according to a linear function, with R^2 of the fit equal to 0.9785.

being mixed with various concentrations of *E. coli* and filtered through a 0.22 μm filter. All absorbance measurements were performed at a measurement wavelength of 450.0 nm, which corresponds to a broad peak in the conjugated CGQDs' absorbance spectrum (Figure S2). As a note, the absorbance peak at approximately 250 nm depicted in Figure 2 could not be examined in this testing method because the compact, portable UV−Vis spectrophotometer used to obtain Figure 6 has a minimum detection wavelength of 380.0 nm, unlike the benchtop UV−Vis spectrometer used to obtain Figure 2.

As can be seen, Figure 6 demonstrates a negative linear relationship between decreases in absorbance and *E. coli* concentration over the *E. coli* concentration range tested (4.45

https://dx.doi.org/10.1021/acsomega.0c03342
ACS Omega XXXX, XXX, XXX−XXX

$\times 10^3$ to 3.62 $\times 10^4$ CFU/mL). Trials performed on different days utilized slightly different concentrations of *E. coli*; therefore, Figure 6 represents the results of six independent trials performed on separate days, with different icons representing data points from different trials. However, aside from *E. coli* concentrations used, these trials were performed under identical experimental conditions.

This negative linear relationship demonstrates that the absorbance of the conjugated CGQDs bound to *E. coli* (absorbance of the filtrate subtracted from control sample absorbance) is directly proportional to the concentration of *E. coli*. Therefore, as *E. coli* concentration increases, the amount of conjugated CGQDs that bind to *E. coli* increases proportionally, and the amount of unbound CGQDs present in the filtrate decreases correspondingly.

Furthermore, our negative linear model for decrease in absorbance versus *E. coli* concentration demonstrated excellent fit with our data, with an R^2 value of 0.9785. Therefore, our assay allows for the precise determination of *E. coli* concentration in a given sample from absorbance measurements.

Meanwhile, Figure 7 depicts the decreases in absorbance that result from nonconjugated CGQDs being mixed with various concentrations of *E. coli* and filtered through a 0.22 μm filter. Figure 7 was obtained under conditions identical to Figure 6, with a measurement wavelength of 450.0 nm. As can be seen when comparing Figures 7 to 6, nonconjugated CGQDs produce much less significant decreases in absorbance compared with conjugated CGQDs. Furthermore, these decreases do not appear to follow the negative linear relationship observed in Figure 6, and rather correlate poorly with such a trend (with an R^2 of just 0.0667). Therefore, the data suggest that conjugation of CGQDs with cecropin P1 appears to be vital for the detection of *E. coli* with our absorbance-based biosensing assay.

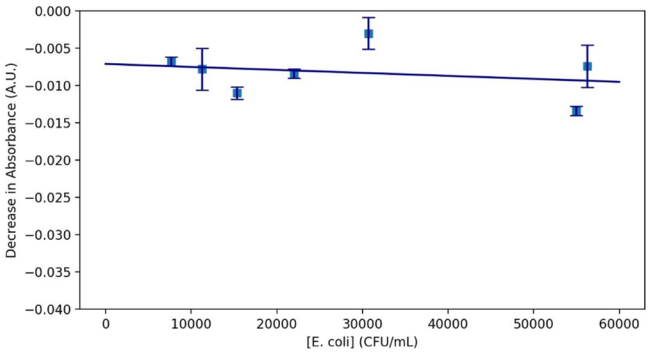

Figure 7. Decrease in the absorbance of nonconjugated CGQDs after being mixed with *E. coli* and filtered through a 0.22 μm filter. Absorbance measurements taken at 450.0 nm. Error bars correspond to the 95% confidence interval of measurements taken on the same sample at five random time points to mitigate the effects of machine uncertainty and random data fluctuations. Curve fitted according to a linear function, with R^2 of the fit equal to 0.0667.

As with our fluorescence-based assay above, it is worth noting that there may be some nonspecific interactions between nonconjugated CGQDs and *E. coli* that may explain some of the absorbance decreases observed in Figure 7 and the seemingly unpredictable nature of these decreases. However, it is clear from the differences between the figures that this random binding is not nearly as significant as that between conjugated CGQDs and *E. coli* cells.

Error bars shown in Figures 6 and 7 represent the 95% confidence intervals of measurements taken on the same sample at five random time points to mitigate the effects of machine uncertainty and random data fluctuations. The *y*-axes of both figures are identically scaled to facilitate direct comparisons between the two.

3. DISCUSSION

3.1. Confirmation of CGQD Conjugation with Cecropin P1. The quenching observed in Figure 1a following CGQD conjugation, as well as the increase in absorbance observed in Figure 2 following conjugation, are hypothesized to be due to aggregation-caused quenching (ACQ), a common phenomenon in quantum dots.[29] In this case, ACQ could result from an increase in conjugated CGQD aggregation due to interactions between the cecropin P1 peptides attached to the CGQDs. Therefore, the observed quenching and increases in absorbance indicate that the CGQDs were successfully conjugated with cecropin P1.

Also suggesting successful conjugation is the 10 nm red shift in absorbance observed following conjugation in Figure 2, which suggests a narrower CGQD band gap as a result of cecropin P1−CGQD binding. Indeed, changes in the band gap have been found to result from the addition of functional groups, as well as other antimicrobial peptides, to quantum dots due to the transfer of charge between quantum dots and the groups added to them.[18,30−32]

Furthermore, the TEM images shown in Figure 3 provide visual evidence that CGQD conjugation has occurred, with Figure 3c showing a CGQD bound to cecropin P1 peptides. The CGQD and peptides in this image are very consistent in size, shape, and coloration with the CGQDs and cecropin P1 peptides shown in Figure 3a and 3b, respectively, and therefore the images collectively suggest the presence of CGQD−cecropin P1 binding following the conjugation protocol.

Finally, comparison of experimental to control tests of our fluorescence-based and absorbance-based biosensing assays, in which conjugated and nonconjugated CGQDs were used (respectively), can be seen in Figures 4−7. These tests further verify the conjugation of our CGQDs with cecropin P1 because replacing conjugated CGQDs with nonconjugated CGQDs leads to an almost complete loss of performance in both of our assays. As both of our assays depend on CGQD−*E. coli* binding for their function, this means that conjugation of our CGQDs with cecropin P1 is essential for the detection of *E. coli* cells. This is an expected outcome considering that cecropin P1 is thought to increase CGQD−*E. coli* binding due to its action mechanism.

3.2. Analysis of Proposed Biosensing Assays. Given cecropin P1's proposed action mechanism of binding to bacterial cell walls, the observed behavior of CGQD fluorescence in Figure 4 is likely due to changes in the CGQD band gap induced by CGQD−*E. coli* binding. The exact nature and cause of these changes in the band gap is unknown as of the writing of this paper, and further investigation is required to explain why CGQD fluorescence increases when CGQD−*E. coli* binding occurs. It is worth noting, however, that the positive relationship between CGQD fluorescence and *E. coli* concentration observed in Figure 4 is similar to that observed in various fluorescence-based, photoluminescence-based, and electrochemiluminescence-

https://dx.doi.org/10.1021/acsomega.0c03342
ACS Omega XXXX, XXX, XXX−XXX

based quantum dot biosensing assays for *E. coli* detection.[9,10,12−17,28]

Meanwhile, the downward linear trend observed in Figure 6 confirms our predictions that the amount of conjugated CGQDs bound to *E. coli* cells following mixing is proportional to *E. coli* concentration, assuming that the absorbance of unbound CGQDs in the filtrate is directly related to unbound CGQD concentration. Furthermore, this confirms our initial assumption that a 0.22 μm filter is able to reliably retain CGQDs bound to *E. coli* while not retaining unbound CGQDs.

For real-world use of our biosensing assays, the fitted curves shown in Figures 4 and 6 can be used as reference curves, so that the *E. coli* concentration of an unknown sample can be determined from the requisite fluorescence and/or absorbance measurements.

3.3. Analysis of LOD and *E. coli* Concentrations Tested. The range of *E. coli* concentrations tested for our fluorescence-based biosensing assay spanned 1.56×10^4 to 1.56×10^6 CFU/mL (as seen in Figure 4). Meanwhile, the range of *E. coli* concentrations tested for our field-deployable, absorbance-based biosensing assay spanned 4.45×10^3 to 3.62×10^4 CFU/mL (as seen in Figure 6). We were able to demonstrate reliable performance of each biosensing assay within these respective concentration ranges. However, these concentration ranges should not be used to define LODs for either biosensing assay, as further testing is needed to quantify detection limits for each.

The ranges of *E. coli* concentrations described above were chosen to mirror concentration ranges of *E. coli* and total coliforms often found in contaminated water sources. Indeed, guidelines for ground, drinking, and tap water quality from various governmental and international bodies (such as the United States EPA and the World Health Organization) suggest that no significant amounts of coliforms should be present in water, with maximum total coliform concentrations commonly equal to 0 CFU/mL.[33,34] However, data from various published studies show that contaminated water sources can have much higher concentrations of *E. coli* and total coliforms, very often ranging from 10^2 to 10^5 CFU/mL in locations such as Lesotho, Gabon, Kenya, Slovakia, Ivory Coast, and Nepal.[35−40]

Therefore, both of our biosensing assays have been demonstrated to detect within real-world *E. coli* and total coliform concentration ranges, specifically on the order of 10^3 to 10^5 CFU/mL. This suggests that the LOD of both biosensing assays is potentially low enough to permit use in real-world applications. Furthermore, both assays' precise quantification of *E. coli* concentration within these ranges may permit their use as simple, rapid tools for assessing water source risk. However, precise quantification of our biosensors' LODs is still needed to see whether lower real-world *E. coli* concentrations (such as those on the order of 10^2 CFU/mL) can also be detected reliably.

4. CONCLUSIONS

Through fluorescence and absorbance spectroscopy, TEM imaging, and analysis of biosensing assay function before and after CGQD conjugation, we have demonstrated the conjugation of CGQDs with the peptide cecropin P1. Furthermore, we have shown that these conjugated CGQDs can be used in two types of biosensing assays to reliably detect the concentration of *E. coli* in solution, within *E. coli* concentration ranges comparable to real-world values observed in contaminated water sources.

These findings hold great potential for fast-acting, practical applications, such as the quantification of bacterial levels in fluids like surface or drinking water. Indeed, our quantum dots were made using nontoxic compounds, important for real-world safety compared to quantum dot biosensors containing heavy metals like cadmium. Additionally, both of our biosensing assays were simple to set up and were not time-intensive, with relatively few experimental steps and the ability to perform fluorescence or absorbance measurements at a given wavelength on the order of 5 min or less (once the conjugated CGQDs were prepared and thoroughly mixed with *E. coli* cells). Finally, our absorbance-based biosensing assay provides a compact, portable, and lower-cost experimental setup for potential field use applications.

We encourage further work to determine the precise LOD of our biosensors and to determine how well our biosensors can detect virulent strains of bacteria such as Shiga toxin-producing *E. coli* O157:H7. Additional methods of confirming CGQD conjugation with cecropin P1 are also encouraged, as well as further analysis of precise CGQD−*E. coli* interactions and the origins of the fluorescence increases observed in Figure 4.

5. EXPERIMENTAL METHODS

5.1. Materials. Graphene quantum dots edge-functionalized with carboxyl groups were obtained from ACS Material (Pasadena, CA) and used as received. Based on technical data provided by ACS Material, the CGQDs ranged in size from 5 to 10 nm and were supplied at a concentration of 1 mg/mL, with a purity of greater than 80%.

Cecropin P1 porcine was obtained from Bachem (Switzerland) and dissolved into sodium acetate buffer (Sigma-Aldrich, 3 M, pH 5.2@25 °C) at a concentration of 1 mg/mL.

NHS and EDC were obtained from Sigma-Aldrich and were each dissolved in sodium acetate buffer at a concentration of 20 mmol/L.

5.2. Conjugation of CGQDs with Cecropin P1. To conjugate CGQDs with the cecropin P1, 60 μL of CGQDs, 60 μL of EDC, and 60 μL of NHS were allowed to react for 30 min at room temperature under mild agitation (provided via an orbital shaker) at 180 rpm. Thereafter, 120 μL of cecropin P1 was added, and the resulting solution was again allowed to react at room temperature under mild agitation at 180 rpm for an additional 2 h. The solution was then diluted with 2100 μL of sodium acetate buffer to give a conjugated CGQD concentration of ∼0.075 mg/mL (∼0.025 mg/mL CGQDs and ∼0.050 mg/mL cecropin P1). The conjugated CGQDs were prepared fresh prior to use in our biosensing assays.

Absorbance and fluorescence spectra of conjugated and nonconjugated CGQDs were taken with a Vernier UV−Vis spectrometer and a Tecan Spark plate reader, respectively, to confirm differences in structural and optical properties associated with conjugation. TEM images of conjugated and nonconjugated CGQDs, as well as cecropin P1, were also obtained with a JEOL JEM-1400 Plus transmission electron microscope in order to confirm CGQD conjugation.

5.3. Preparation of *E. coli* Liquid Cultures. The bacteria used in this study were cultured in Luria−Bertani medium from competent K12 *E. coli* DH5-α cells. Only cells with no antibiotic resistance and no added genetic modifications were tested in this study. This was done to minimize the

https://dx.doi.org/10.1021/acsomega.0c03342
ACS Omega XXXX, XXX, XXX−XXX

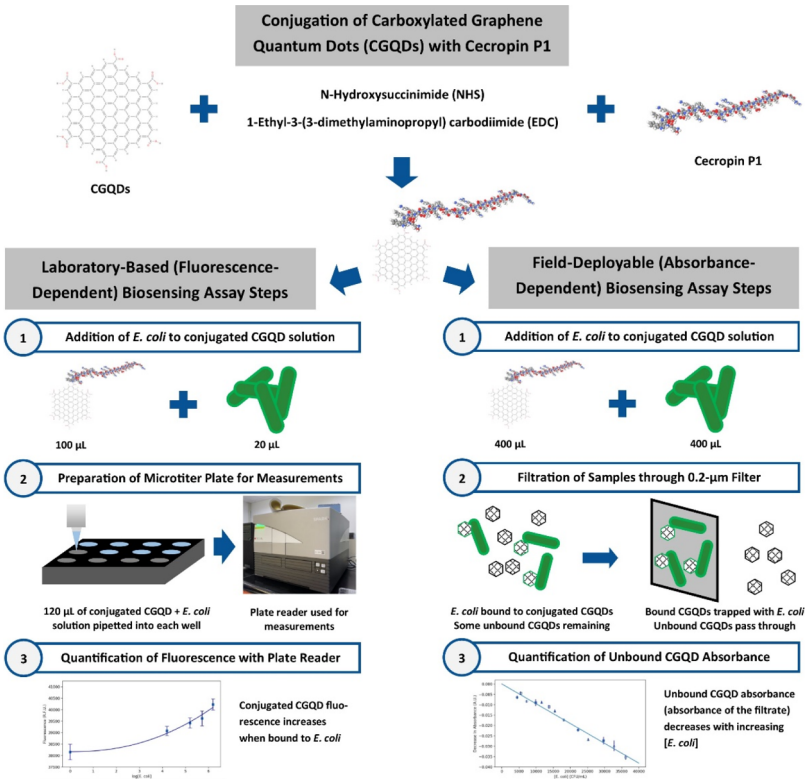

Figure 8. Scheme of mechanism and experimental steps for conjugation protocol as well as fluorescence-based and absorbance-based biosensing assays.

interference of additional cell surface proteins with *E. coli*–CGQD binding.

Prior to using our *E. coli* liquid cultures to test our fluorescence-based and absorbance-based biosensing assays, our cells were resuspended in sodium acetate buffer (Sigma-Aldrich). This was done to eliminate any effects of the Luria–Bertani medium on our absorbance and fluorescence measurements. Then, the concentration of our resuspended *E. coli* cells was quantified via OD_{600} measurements taken with a Vernier SpectroVis spectrophotometer, and dilutions of the resuspended cells to various concentrations were performed for use in our biosensing assays.

5.4. Procedure for a Laboratory-Based Biosensing Assay. To create a laboratory-based biosensing assay, we mixed our conjugated CGQDs and resuspended *E. coli* liquid cultures in a black 96-well microtiter plate and performed fluorescence intensity measurements using a Tecan Spark plate reader. Into each well of the microtiter plate, we pipetted 100 μL of conjugated CGQDs and 20 μL of *E. coli* liquid culture of varying concentrations. A well with 100 μL of conjugated CGQDs mixed with 20 μL of sodium acetate buffer was also examined as a negative control. Upon loading all solutions, we thoroughly agitated the contents of each well to ensure complete *E. coli*–CGQD binding before performing fluorescence intensity measurements. The scheme illustrated in Figure 8 provides a visual illustration of this preparation protocol.

Using these measurements, we analyzed how changes in *E. coli* concentration affected the fluorescence of the CGQD–*E. coli* mixture (Figure 4).

5.5. Procedure for an Absorbance-Based Biosensing Assay. For each concentration of *E. coli* tested with our absorbance-based assay, we thoroughly mixed 400 μL of conjugated CGQDs with 400 μL of resuspended *E. coli* liquid culture for 5 min, ensuring that all possible *E. coli*–CGQD binding occurred. Following mixing, we filtered the resulting solution using a 0.22 μm filter; conjugated CGQDs alone are too small in size to be trapped by the filter, but conjugated CGQDs bound to *E. coli* cells are trapped in the filter with the *E. coli*. With only unbound CGQDs remaining in the filtrate, we then obtained an absorbance measurement of the filtrate at 450.0 nm using a Vernier SpectroVis spectrophotometer (this was not the same as the Vernier UV–Vis spectrometer used to obtain Figure 2, but rather a more compact and portable model). A control sample containing 400 μL of conjugated CGQDs and 400 μL of sodium acetate buffer was mixed, filtered, and analyzed according to the same protocol. The scheme illustrated in Figure 8 provides a visual illustration of this preparation protocol.

After obtaining the absorbance measurements described above, we analyzed the differences between the OD_{450} of the control sample and the OD_{450} of samples associated with different *E. coli* concentrations. Decreases in OD_{450} relative to the control were then plotted against *E. coli* concentration (Figure 6).

■ ASSOCIATED CONTENT

Supporting Information

The Supporting Information is available free of charge at https://pubs.acs.org/doi/10.1021/acsomega.0c03342.

Absorbance spectrum of pure cecropin P1, including a comparison with the absorbance spectra of non-conjugated CGQDs and conjugated CGQDs. Absorbance spectrum of CGQDs conjugated with cecropin P1,

https://dx.doi.org/10.1021/acsomega.0c03342
ACS Omega XXXX, XXX, XXX–XXX

measured from 380.0 to 550.0 nm with a Vernier SpectroVis portable spectrophotometer (PDF)

AUTHOR INFORMATION

Corresponding Author

Jonathan A. Bruce − *Taipei American School, Taipei 11152, Taiwan;* orcid.org/0000-0002-9906-6995; Email: jbruce1461@gmail.com

Author

Jude C. Clapper − *Taipei American School, Taipei 11152, Taiwan*

Complete contact information is available at: https://pubs.acs.org/10.1021/acsomega.0c03342

Author Contributions

J.A.B.: conceptualization, methodology & data curation, investigation, validation, formal analysis, visualization, and writing—original draft & editing. J.C.C.: writing—review & editing, funding acquisition, supervision & resources, and project administration.

Funding

This research was funded by the Taipei American School. The funders had no role in study design, data collection and analysis, decision to publish, or preparation of the manuscript.

Notes

The authors declare no competing financial interest.

ACKNOWLEDGMENTS

The authors are grateful to Dr. Wan-Chun Li and Yi-Ta Hsieh of National Yang Ming University, School of Dentistry, for granting access to their plate reader and TEM, as well as offering advice on these methods of sample analysis. The authors thank Sean Tsao of Taipei American School for resources.

REFERENCES

(1) Ahmed, A.; Rushworth, J. V.; Hirst, N. A.; Millner, P. A. Biosensors for whole-cell bacterial detection. *Clin. Microbiol. Rev.* **2014**, *27*, 631−646.

(2) Kumar, N.; Hu, Y.; Singh, S.; Mizaikoff, B. Emerging biosensor platforms for the assessment of water-borne pathogens. *Analyst* **2018**, *143*, 359−373.

(3) Leonard, P.; Hearty, S.; Brennan, J.; Dunne, L.; Quinn, J.; Chakraborty, T.; O'Kennedy, R. Advances in biosensors for detection of pathogens in food and water. *Enzym. Microb. Technol.* **2003**, *32*, 3−13.

(4) Lim, J. Y.; Yoon, J.; Hovde, C. J. A brief overview of Escherichia coli O157:H7 and its plasmid O157. *J. Microbiol. Biotechnol.* **2010**, *20*, 5−14.

(5) Lin, F.; Bao, Y.-W.; Wu, F.-G. Carbon dots for sensing and killing microorganisms. *C* **2019**, *5*, 33.

(6) Mazumder, S.; Dey, R.; Mitra, M.-K.; Mukherjee, S.; Das, G.-C. Review: biofunctionalized quantum dots in biology and medicine. *J. Nanomater.* **2009**, *2009*, 815734.

(7) Zhong, M.; Yang, L.; Yang, H.; Cheng, C.; Deng, W.; Tan, Y.; Xie, Q.; Yao, S. An electrochemical immunobiosensor for ultrasensitive detection of Escherichia coli O157:H7 using CdS quantum dots-encapsulated metal-organic frameworks as signal-amplifying tags. *Biosens. Bioelectron.* **2019**, *126*, 493−500.

(8) Su, X.-L.; Li, Y. Quantum Dot Biolabeling Coupled with Immunomagnetic Separation for Detection of Escherichia coli O157:H7. *Anal. Chem.* **2004**, *76*, 4806−4810.

(9) Chen, S.; Chen, X.; Zhang, L.; Gao, J.; Ma, Q. Electrochemiluminescence detection of Escherichia coli O157:H7 based on a novel polydopamine surface imprinted polymer biosensor. *ACS Appl. Mater. Interfaces* **2017**, *9*, 5430−5436.

(10) Bae, P. K.; So, H.-M.; Kim, K. N.; You, H. S.; Choi, K. S.; Kim, C. H.; Park, J.-K.; Lee, J.-O. Simple route for the detection of Escherichia coli using quantum dots. *Biochip J.* **2010**, *4*, 129−133.

(11) Yu, J.; Su, J.; Zhang, J.; Wei, X.; Guo, A. CdTe/CdS quantum dot-labeled fluorescent immunochromatography test strips for rapid detection of Escherichia coli O157:H7. *RSC Adv.* **2017**, *7*, 17819−17823.

(12) Demirkol, D. O.; Timur, S. A sandwich-type assay based on quantum dot/aptamer bioconjugates for analysis of E. coli O157:H7 in microtiter plate format. *Int. J. Polym. Mater. Polym. Biomater.* **2016**, *65*, 85−90.

(13) Weng, C.-I.; Chang, H.-T.; Lin, C.-H.; Shen, Y.-W.; Unnikrishnan, B.; Li, Y.-J.; Huang, C.-C. One-step synthesis of biofunctional carbon quantum dots for bacterial labeling. *Biosens. Bioelectron.* **2015**, *68*, 1−6.

(14) Chandra, S.; Mahto, T. K.; Chowdhuri, A. R.; Das, B.; Sahu, S. K. One step synthesis of functionalized carbon dots for the ultrasensitive detection of Escherichia coli and iron (III). *Sens. Actuators, B* **2017**, *245*, 835−844.

(15) Chandra, S.; Chowdhuri, A. R.; Mahto, T. K.; Samui, A.; Sahu, S. K. One-step synthesis of amikacin modified fluorescent carbon dots for the detection of Gram-negative bacteria like Escherichia coli. *RSC Adv.* **2016**, *6*, 72471−72478.

(16) Bhaisare, M. L.; Gedda, G.; Khan, M. S.; Wu, H.-F. Fluorimetric detection of pathogenic bacteria using magnetic carbon dots. *Anal. Chim. Acta* **2016**, *920*, 63−71.

(17) Sanvicens, N.; Pascual, N.; Fernández-Argüelles, M. T.; Adrián, J.; Costa-Fernández, J. M.; Sánchez-Baeza, F.; Sanz-Medel, A.; Marco, M.-P. Quantum dot-based array for sensitive detection of Escherichia coli. *Anal. Bioanal. Chem.* **2011**, *399*, 2755−2762.

(18) Carrillo-Carrión, C.; Simonet, B. M.; Valcárcel, M. Colistin-functionalised CdSe/ZnS Quantum Dots as Fluorescent Probe for the Rapid Detection of Escherichia Coli. *Biosens. Bioelectron.* **2011**, *26*, 4368−4374.

(19) Chen, N.; He, Y.; Su, Y.; Li, X.; Huang, Q.; Wang, H.; Zhang, X.; Tai, R.; Fan, C. The cytotoxicity of cadmium-based quantum dots. *Biomaterials* **2012**, *33*, 1238−1244.

(20) Contreras, E. Q.; Cho, M.; Zhu, H.; Puppala, H. L.; Escalera, G.; Zhong, W.; Colvin, V. L. Toxicity of quantum dots and cadmium salt to Caenorhabditis elegans after multigenerational exposure. *Environ. Sci. Technol.* **2013**, *47*, 1148−1154.

(21) Sharma, V. K.; McDonald, T. J.; Sohn, M.; Anquandah, G. A. K.; Pettine, M.; Zboril, R. Assessment of toxicity of selenium and cadmium selenium quantum dots: a review. *Chemosphere* **2017**, *188*, 403−413.

(22) Wang, S.; Cole, I. S.; Li, Q. The toxicity of graphene quantum dots. *RSC Adv.* **2016**, *6*, 89867−89878.

(23) Zhu, S.; Song, Y.; Wang, J.; Wan, H.; Zhang, Y.; Ning, Y.; Yang, B. Photoluminescence mechanism in graphene quantum dots: Quantum confinement effect and surface/edge state. *Nano Today* **2017**, *13*, 10−14.

(24) Fan, Z.; Li, S.; Yuan, F.; Fan, L. Fluorescent graphene quantum dots for biosensing and bioimaging. *RSC Adv.* **2015**, *5*, 19773−19789.

(25) Steiner, H.; Andreu, D.; Merrifield, R. B. Binding and Action of Cecropin and Cecropin Analogues: Antibacterial Peptides from Insects. *Biochim. Biophys. Acta, Biomembr.* **1988**, *939*, 260−266.

(26) Boman, H. G.; Agerberth, B.; Boman, A. Mechanisms of Action on Escherichia Coli of Cecropin P1 and PR-39, Two Antibacterial Peptides From Pig Intestine. *Infect. Immun.* **1993**, *61*, 2978−2984.

(27) Han, F.-F.; Liu, Y.-F.; Xie, Y.-G.; Gao, Y.-H.; Luan, C.; Wang, Y.-Z. Antimicrobial peptides derived from different animals: comparative studies of antimicrobial properties, cytotoxicity and mechanism of action. *World J. Microbiol. Biotechnol.* **2011**, *27*, 1847−1857.

(28) Herman, R. A.; Scherer, P. N.; Shan, G. Evaluation of logistic and polynomial models for fitting sandwich-ELISA calibration curves. *J. Immunol. Methods* **2008**, *339*, 245−258.
(29) Wang, N.; Liu, Z. X.; Li, R. S.; Zhang, H. Z.; Huang, C. Z.; Wang, J. The aggregation induced emission quenching of graphene quantum dots for visualizing the dynamic invasions of cobalt(ii) into living cells. *J. Mater. Chem. B* **2017**, *5*, 6394−6399.
(30) Li, Y.; Shu, H.; Niu, X.; Wang, J. Electronic and optical properties of edge-functionalized graphene quantum dots and the underlying mechanism. *J. Phys. Chem. C* **2015**, *119*, 24950−24957.
(31) He, X.; Gao, L.; Ma, N. One-step instant synthesis of protein-conjugated quantum dots at room temperature. *Sci. Rep.* **2013**, *3*, 2825.
(32) Sahoo, S. L.; Liu, C.-H.; Kumari, M.; Wu, W.-C.; Wang, C.-C. Biocompatible quantum dot-antibody conjugate for cell imaging, targeting and fluorometric immunoassay: crosslinking, characterization and applications. *RSC Adv.* **2019**, *9*, 32791−32803.
(33) National Primary Drinking Water Regulations—Ground Water and Drinking Water. United States Environmental Protection Agency Web site. https://www.epa.gov/ground-water-and-drinking-water/national-primary-drinking-water-regulations (accessed Sep 10, 2020).
(34) International Comparison of Water Quality. Taipei Water Department Web site. https://english.water.gov.taipei/cp.aspx?n=ED0C1E259A61491D (accessed Sep 10, 2020).
(35) Gwimbi, P.; George, M.; Ramphalile, M. Bacterial contamination of drinking water sources in rural villages of Mohale Basin, Lesotho: exposures through neighbourhood sanitation and hygiene practices. *Environ. Health Prev. Med.* **2019**, *24*, 33.
(36) Ehrhardt, J.; Alabi, A.-S.; Kremsner, P.-G.; Rabsch, W.; Becker, K.; Foguim, F.-T.; Kuczius, T.; Esen, M.; Schaumburg, F. Bacterial contamination of water samples in Gabon, 2013. *J. Microbiol., Immunol. Infect.* **2017**, *50*, 718−722.
(37) Onyango, A. E.; Okoth, M. W.; Kunyanga, C. N.; Aliwa, B. O. Microbiological quality and contamination level of water sources in Isiolo County in Kenya. *J. Environ. Public Health* **2018**, *2018*, 2139867.
(38) Sasakova, N.; Gregova, G.; Takacova, D.; Mojzisova, J.; Papajova, I.; Venglovsky, J.; Szaboova, T.; Kovacova, S. Pollution of surface and ground water by sources related to agricultural activities. *Front. Sustain. Food Syst.* **2018**, *2*, 42.
(39) Lavoie, M. C.; Viens, P. Water quality control in rural Ivory Coast. *Trans. R. Soc. Trop. Med. Hyg.* **1983**, *77*, 119−120.
(40) Haramoto, E.; Yamada, K.; Nishida, K. Prevalence of protozoa, viruses, coliphages and indicator bacteria in groundwater and river water in the Kathmandu Valley, Nepal. *Trans. R. Soc. Trop. Med. Hyg.* **2011**, *105*, 711−716.

https://dx.doi.org/10.1021/acsomega.0c03342
ACS Omega XXXX, XXX, XXX−XXX